CCFE
CULHAM CENTRE FOR FUSION ENERGY

UK Atomic Energy Authority

UKAEA-CCFE-PR(21)79

J. W. Berkery, S. A. Sabbagh, L. Kogan, D. Ryan, J. M. Bialek, Y. Jiang, D. J. Battaglia, S. Gibson, C. Ham

# Kinetic Equilibrium Reconstructions of Plasmas in the MAST Database and Preparation for Reconstruction of the First Plasmas in MAST Upgrade

# Kinetic Equilibrium Reconstructions of Plasmas in the MAST Database and Preparation for Reconstruction of the First Plasmas in MAST Upgrade

J. W. Berkery, S. A. Sabbagh, L. Kogan, D. Ryan, J. M. Bialek, Y. Jiang, D. J. Battaglia, S. Gibson, C. Ham

This is a preprint of a paper submitted for publication in Plasma Physics and Controlled Fusion

# Kinetic Equilibrium Reconstructions of Plasmas in the MAST Database and Preparation for Reconstruction of the First Plasmas in MAST Upgrade

**J W Berkery[1], S A Sabbagh[1], L Kogan[2], D Ryan[2], J M Bialek[1], Y Jiang[1], D J Battaglia[3], S Gibson[4], C Ham[2]**

[1] Department of Applied Physics and Applied Mathematics, Columbia University, New York, New York 10027, USA
[2] Culham Centre for Fusion Energy, UKAEA, Abingdon, OX14 3DB, UK
[3] Princeton Plasma Physics Laboratory, Princeton, New Jersey, 08543, USA
[4] Centre for Advanced Instrumentation, Durham University, Durham, DH1 3LE, UK

E-mail: jberkery@pppl.gov

Received xxxxxx
Accepted for publication xxxxxx
Published xxxxxx

## Abstract

Reconstructions of plasma equilibria using magnetic sensors and a Dα constraint were routine during operation of the MAST spherical tokamak, but reconstructions using kinetic profiles was not. These are necessary for stability and disruption analysis of the MAST database, as well as going forward for operation in the upgrade to the device, MAST-U. The three dimensional code VALEN is used to determine eddy currents in the 3D vessel structures for vacuum coil test shots, which are then mapped to effective resistances in the 2D vessel groupings in the EFIT equilibrium reconstruction code to be used in conjunction with nearby loop voltage measurements for estimated currents in the structures during reconstruction. Kinetic equilibrium reconstructions with EFIT, using all available magnetic sensors as well as Thomson scattering measurements of electron temperature and density, charge exchange recombination spectroscopy measurements of ion temperature, and internal magnetic field pitch angle measurements from a motional Stark effect (MSE) diagnostic are performed for a large database of MAST discharges. Excellent convergence errors are obtained for the portions of the discharges where the stored energy was not too low, and it is found that reconstructions performed with temperature and density measurements but without MSE data usually already match the pitch angle measurements well; adding MSE data corroborates, but generally does not substantially change, the reconstructions. A database of 275 kinetic equilibria is used to test the ideal MHD stability calculation capability for MAST. Finally, the necessary changes to conducting structure in VALEN, and diagnostic setup in EFIT have been completed for the upgrade from MAST to MAST-U, enabling kinetic reconstructions to commence from the first plasma discharges of the upgraded device.

Keywords: equilibrium reconstruction, stability, spherical tokamak

(Some figures may appear in colour only in the online journal)

## 1. Introduction

The MAST spherical tokamak experiment was a low aspect ratio fusion plasma device [1]. Currently an upgrade to the device, called MAST-U [2], has begun operation. Accurate reconstruction of the plasma equilibrium state from various diagnostic measurements is crucial for the operation of MAST-U, as well as for the majority of plasma physics analyses including the stability analyses and disruption event characterization and forecasting [3,4]. These last applications

 

require *kinetic* equilibrium reconstructions, that is to say reconstructions using available measurements of the plasma pressure, for high accuracy.

Magnetic, kinetic, and rotating equilibrium reconstruction for low aspect ratio ST plasmas has long been demonstrated [5]. MAST had, and MAST-U continues to have, world-class high resolution Thomson scattering measurements of electron temperature and density as well as charge exchange recombination spectroscopy measurements of ion temperature required for kinetic reconstructions. In the present work, ion density and energetic particle pressure profiles are modelled to obtain the total pressure. Internal magnetic field pitch angle measurements from motional Stark effect (MSE) diagnosis are also included for accurate determination of the safety factor, $q$, profile. The equilibrium reconstructions also include fitting of field shaping coil currents, and wall vessel currents (a critical component of reconstructions in low $A$ plasmas due to the close presence of conducting elements in the device).

Reconstructions using a partial set of the magnetic measurements available during MAST operation, as well as a constraint on the last closed flux surface of the plasma through an optical measurement of Dα radiation [6], were previously performed for each MAST discharge. These could then be used for database studies (as one example, see Ref. [7]). Reconstructions beyond magnetics-only were later performed individually for specialized studies, but were not uniformly available for the MAST database. For example, a limited number of kinetic equilibrium reconstructions with partial electron and ion pressure constraints and modelled fast ion pressures have been previously performed for MAST [8], but MSE measurements were not available at that time. Later, MSE was used to constrain the $q$ profile for reconstructions otherwise using the inboard magnetics, but not the outboard magnetics or kinetic profiles [9]. A Bayseian inference technique was also pursued to compute MAST equilibria [10]. Finally, all diagnostics were brought together through a code suite called MC$^3$, which included magnetics, MSE, and finally total pressure, using the TRANSP particle transport analysis code [11] to determine the fast ion pressure component [12,13,14]. This level of equilibrium reconstruction was not routine, however, for MAST, and the present work aims to make it routine for re-examination of the MAST database of discharges, as well as going forward for operation of MAST-U. Additionally, the magnetics only level of reconstruction is recomputed here by using all available magnetics and no boundary constraint.

In section 2 the general concept of tokamak plasma equilibrium reconstruction is briefly reviewed, along with the specific equations solved here with various levels of diagnostic inclusion. Modelling of the conducting structure surrounding the plasmas in the MAST device is discussed in section 3, with consideration of how this modelling leads to estimated induced currents in vessel segments which are then used in the reconstructions. The resulting reconstructions using magnetics only, kinetic, or kinetic plus MSE for MAST are compared in section 4 and used as a database for stability calculations in section 5. Finally, preparations for reconstruction of the first plasmas from MAST-U are outlined in section 6 and conclusions of the study are drawn.

## 2. Equilibrium reconstruction

A fusion plasma is in equilibrium when a steady-state force balance is in effect. The state of this equilibrium for a given discharge at a given time can be reconstructed from various measurements and this provides profiles of various plasma parameters, such as pressure. The EFIT code is an equilibrium reconstruction code for tokamak plasmas [15,16,17]. While one particular implementation of the EFIT code, called EFIT++, has been used for MAST reconstructions in the past [18], another implementation, previously used for the NSTX [5] and KSTAR [19] devices, is now being used for MAST reconstructions in the present work. Both of these codes will be used for MAST-U operation, as will be discussed in section 6.

The equilibrium of a tokamak plasma satisfies a balance of current and pressure forces, $\nabla p = j \times B$. In two dimensional axisymmetry, this results in the Grad-Shafranov equation,

$$R^2\nabla\cdot\left(\frac{\nabla\psi}{R^2}\right) = -\mu_0 R J_\varphi,$$

where the toroidal plasma current is defined by,

$$\mu_0 J_\varphi = \mu_0 R\frac{\partial p}{\partial\psi} + \frac{f}{R}\frac{\partial f}{\partial\psi},$$

with $p$ the total plasma pressure and $f = RB_\varphi$. Reconstruction of the plasma equilibrium requires the specification of two functions. Normally one selects $\partial p/\partial\psi$ and $f\partial f/\partial\psi$.

The function $f\partial f/\partial\psi$ is assumed to be a function of $\psi_N$ only, where $\psi_N$ is the flux normalized so that it spans 0:1 from axis to edge. We use a polynomial basis set of order $n_f$ to specify $f\frac{\partial f}{\partial\psi} = \sum_0^{n_f}\gamma_n\psi_N^n$, and at this point a constraint is placed on the equation. We use the constraint that the derivative of $f\partial f/\partial\psi$ is zero at the edge,

$$\left[\frac{\partial}{\partial\psi}\left(f\frac{\partial f}{\partial\psi}\right)\right]_{\psi_n=1} = 0\,.$$

This can be achieved by stipulating that the $\gamma$ parameters should abide by the constraint $C_0\sum_1^{n_f} n\gamma_n = 0$, where $C_0$ is an arbitrary constant. This same constraint on $f\partial f/\partial\psi$ is used in all levels of reconstruction. When a constraint is applied in the EFIT code, it is by adding an additional equation to the system that is solved by least squares regression, and that

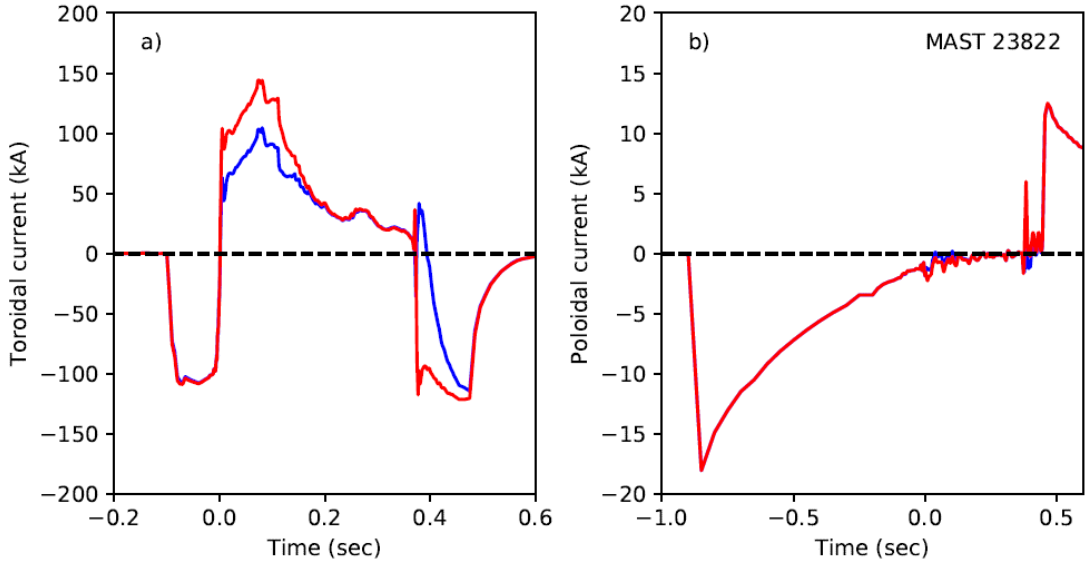


**Figure 1.** (a) Total induced toroidal current and (b) poloidal current in the MAST conducting structure with (blue) and without (red) plasma current for discharge 23822, as calculated by VALEN. Note the different time and current scales for each plot.

equation is given a weight. The constraint, despite its name, is therefore not strictly enforced, although it can be effectively made to be by giving a sufficient weight.

The second function, the pressure gradient $\partial p/\partial\psi$, is also treated as a polynomial of order $n_p$: $\frac{\partial p}{\partial \psi} = \sum_0^{n_p} \alpha_n \psi_N^n$, and similarly, a constraint is placed on this equation. We set the pressure gradient at the axis equal to zero, so that $\alpha_0 \approx 0$.

The two functions are treated with varying polynomial orders $n_f$ and $n_p$, as well as one additional constraint at the kinetic reconstruction level, leaving different numbers of free parameters, depending on the measurements used as inputs. Selection of the polynomial orders is a tradeoff between a larger value allowing more detail in the profiles but also introducing more unknowns to the reconstruction, potentially increasing the convergence error. Each level of analysis will now be described in detail.

### *2.1 Magnetics only reconstruction*

Magnetic diagnostics [20] are used in all levels of equilibrium reconstruction. At its most basic level, the EFIT code can use magnetics data only, without any direct measurement of the pressure profile. The MAST device was fully equipped with magnetic diagnostics, including Rogowski coils, pickup coils, and flux loops [21].

In the magnetics only case, because no pressure measurements are available, we treat the total plasma pressure gradient as a polynomial flux function with the relatively simple order of $n_p$ = 2. Additionally, because we have specified a pressure gradient of zero at the axis, we can reduce the expression to $\partial p/\partial\psi \approx \alpha_1\psi_N + \alpha_2\psi_N^2$, and for the magnetics only reconstruction we will also specify a pressure gradient of zero at the edge. We then fit $\partial p/\partial\psi$ to,

$$\frac{\partial p}{\partial \psi} \approx \alpha_1 \psi_n (1 - \psi_n),$$

and the resulting pressure profile conforms to

$$p \approx p_0\left(1 - 3{\psi_n}^2 + 2{\psi_n}^3\right),$$

where $p_0$ is the pressure on axis.

In the magnetics only reconstruction, the order for $f\partial f/\partial\psi$ of $n_f$ =4 is used, without additional constraints, besides the derivative of $f\partial f/\partial\psi$ equal to zero at the edge listed above.

### *2.2 Partial kinetic reconstruction*

In addition to magnetics data, the next level of reconstruction uses the Thomson scattering profiles of electron density and temperature [22,23], and the charge exchange recombination spectroscopy profile of ion temperature [24] to partially constrain the pressure profile [16]. This reconstruction is called "partial kinetic" because the ion density and the fast particle pressure are not measured. In this case, the ion density is assumed to be equal to the electron density times a constant less than one – here we found 0.7 to give good results – to account for the presence of impurity ions. The ion pressure is given a substantial error bar in the fitting procedure because of the uncertainty due to this assumption. A trustworthy measurement of the plasma effective charge state, $Z_{eff}$ [25],

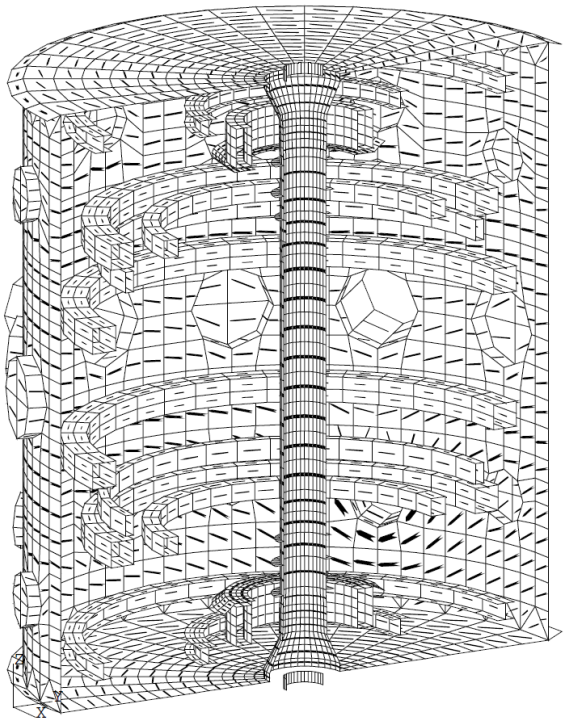

**Figure 2.** View of the eddy current pattern in the MAST conducting structure during plasma discharge 23822.

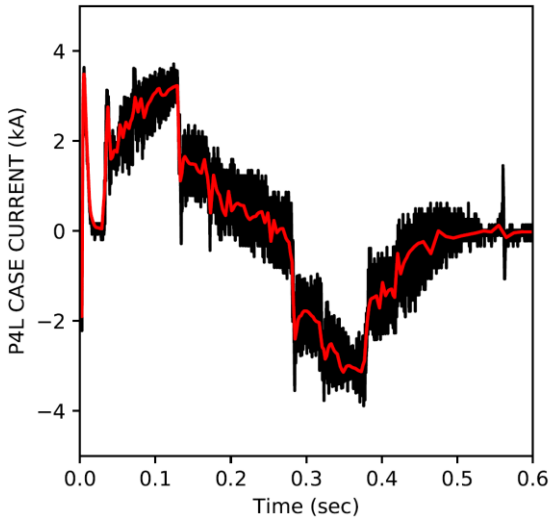


**Figure 3.** Comparison between measured (black) and VALEN modelled (red) induced currents in the lower P4 coil case during MAST poloidal field coil test discharge 23588.

would be useful to give a better estimate of ion density. The fast particle pressure, which can also constitute a significant portion of the total pressure, is here modelled to be equal to the electron pressure, also with a large error bar. Reconstruction with this partial level of kinetic measurement input, however, is commonly referred to simply as kinetic reconstruction.

As mentioned, assumed "measured" profiles of ion and fast particle pressures are used, with large error bars to allow flexibility in the total pressure profile. It would also be possible to couple the reconstruction to a transport code [26], or to use the original equilibrium as an input to a transport calculation which provides a calculated $p_f$ profile. Then this profile could be used as a "measured" input (again with large error bars because it is not a truly measured quantity) in the equilibrium reconstruction, and the process could be iterated until reasonable convergence is obtained. Alternatively, a neural network emulation of the results of TRANSP calculations could also be used to model the fast ion pressure [27]. These steps have not yet been taken in the present analysis.

Because the pressure profile is being constrained by more measurements, it is possible to give more freedom to the fit for $\partial p/\partial\psi$. For all kinetic reconstructions, we have used a polynomial order of five and the zero gradient constraint at the axis (but not at the edge, like in the magnetics only case). The weight on this pressure gradient constraint is not large, and in the cases shown here the solution often does not obey it, resulting in a gradient at the axis.

Finally, we also used $n_f = 5$ for $f\partial f/\partial\psi$, but in addition to the previously described constraint, we now also specify that the value of $f\partial f/\partial\psi$ is zero on axis,

$$\left[f\frac{\partial f}{\partial\psi}\right]_{\psi_n=0} = 0\,,$$

which is achieved by setting $\gamma_0 \approx 0$.

### *2.3 Partial kinetic reconstruction with MSE*

Besides the density and temperature measurement inputs, at this stage of reconstruction, magnetic field pitch angle data, measured by the motional Stark effect (MSE) diagnostic, can also be used. The motional Stark effect diagnostic for MAST [28,29] is used to find the polarization angle of light emitted from neutral beam particles in the local magnetic field of the plasma. The polarization angle is self-consistently converted to the magnetic pitch angle using the magnetic field components during the iterative steps of our equilibrium reconstruction. Naturally, the magnetic pitch angle measurement, the only magnetic measurement internal to the plasma, serves as a strong constraint on the $q$ profile in the plasma, $q$ being a measure of the ratio of different magnetic field components. Adding MSE provides a better constraint to the equilibrium reconstruction, but no changes to the order or constraints for $\partial p/\partial\psi$ or $f\partial f/\partial\psi$ are made at this step.

MSE-constrained equilibria are important especially for MHD stability studies, in which case knowledge of the $q$ profile, and especially $q_0$ is critical. An example from MAST is the study

of the so-called long lived mode, which evolves as $q_0$ approaches, but stays above, one [9].

Finally, reconstructions including plasma rotation are also possible [17,30,31,32,33], but have not been performed for MAST or MAST-U plasmas in this work. For MAST, it has been speculated that disagreement between inboard and outboard temperature and density profiles could be indicating a rotational shift of the flux surfaces [8]. Indeed, the importance of flow in radial force balance was previously demonstrated for a single MAST discharge/time point [31]. The measurement capabilities do make this level of analysis possible, and the generally high levels of toroidal rotation in spherical tokamaks with neutral beam injection providing torque [34] makes it worthy of consideration for future work.

## 3. Modelling of the MAST conducting structure supporting equilibrium analysis

For equilibrium analyses of spherical tori it is important to include currents in the conducting structure of the tokamak modelled, as their influence will dominate the toroidal current during plasma current ramp-up, and will comprise a significant component of the plasma current well into the $I_p$ flat-top period of the discharge. To obtain the best set of effective resistances of the wall segments for equilibrium reconstruction, we have created a 3D non-axisymmetric model of the wall, including the center column, the coil cases, and the vacuum vessel with ports, using the VALEN code [35]. The VALEN code approximates the conducting structure surrounding the plasma by splitting a thin-shell into finite elements which are each mutually coupled to all other elements in the model. Then, when some currents in the system are specified, currents that are induced in the conducting structure can be identified.

As a first test of this capability for MAST, time-domain calculations were performed using experimental currents in coils with and without plasma current for MAST discharge 23822. As an approximation, the plasma current was uniformly distributed in a circular cross section at the experimental major and minor radius. Figure 1 shows the resulting net toroidal and poloidal currents in the conducting structure of MAST. As expected, the toroidal current in the conducting structure is reduced when plasma current is present. For comparison, the flat-top plasma current in this discharge was ~750 kA, so the induced current is significant. The toroidal current is induced by the changing poloidal field coil currents, especially the +22 to -17 kA swing in the P1 Ohmic solenoid in the centre case. The much smaller (note the scale in Fig. 1b) poloidal conducting structure current, which is essentially zero during the plasma discharge time of ~0 to 0.4 s, is induced by the slower toroidal field coil current ramp to and from -86 kA. Figure 2 shows the eddy current pattern of current in the MAST conducting structure when the plasma is present and the toroidal current dominates. The size of the arrows indicates the strength of the current in each segment of the structure. One can see the pattern of the current is mostly toroidal, with some current flowing around vacuum ports.

Measurements of the currents in some plasma facing wall components, namely the coil cases, were available during MAST operation. These were measured by the difference between Rogowski coil measurements of the current through the coils plus cases, and the coils alone, measured at the leads. An example of a comparison between these measured currents and the current isolated to that particular coil case in the VALEN model is shown in Fig. 3.

The close match of the coil case current comparison gives confidence in the VALEN model. That model is now used to approximate the current in other, unmeasured, vessel segments for the equilibrium reconstruction. A similar, though strictly two-dimensional, procedure was previously used for MAST reconstructions [36]. First, we have divided the MAST

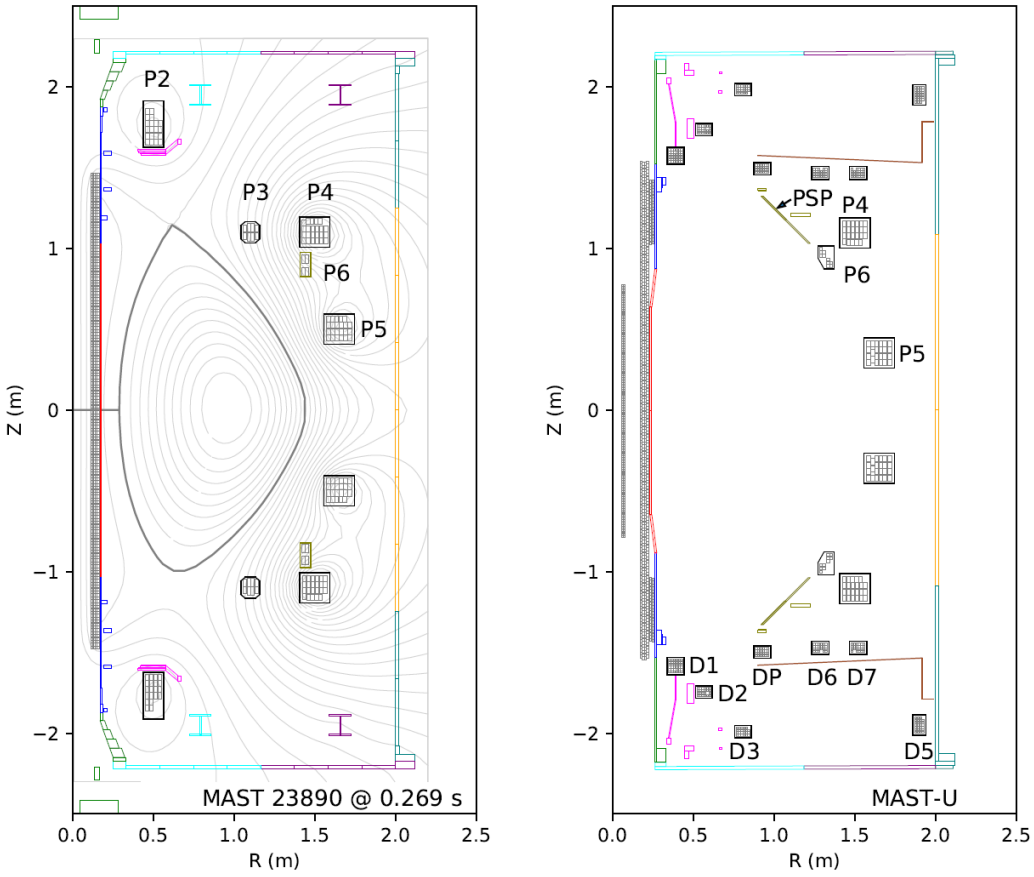


**Figure 4.** Diagrams of (left) MAST, and (right) MAST-U poloidal field coils (grey), their cases (black), and all toroidally continuous conducting vessel structures (colours), as well as the flux surfaces of an example plasma equilibrium reconstruction. There are a total of 18 vessel segments in the MAST model, including the P6 cases and the divertor plates near P2. There are 20 for MAST-U including the colosseum structure outside of D1-3, the gas baffle outside of DP6-7, and the passive stabilization plates between DP and P6. Colours are reused for upper and lower segments to show symmetry, but these segments are considered separately, including two inner wall segments in red and two outer wall segments in orange, each split at the midplane into upper and lower parts.

conducting structure into 14 axisymmetric toroidal segment groupings, plus an upper and lower divertor plate near poloidal field coils P2. Additionally, the P6 coil cases are treated as vessel segments, as their currents were not measured. This total of 18 vessel segments without experimentally measured current is shown in Fig. 4a (the flux surfaces from an equilibrium reconstruction are also included – these will be discussed in section 4, and the MAST-U diagram in Fig. 4b will be discussed in section 5). Only stainless steel and Inconel components are shown, carbon tiles are not. There is a tradeoff between having too few or too many modelled vessel segments. Too few will mean that the reconstruction cannot sufficiently capture the distribution of current in the vessel to accurately match the magnetics, while too many gives the equilibrium reconstruction too much freedom to distribute the current, resulting in degenerate solutions.

By grouping the VALEN elements into the same segments, the total induced current flowing in each of those segments can be determined. While, theoretically, one could run VALEN iteratively as a part of the reconstruction of each discharge, using the modelled currents in the vessel segments from VALEN directly, it is much more practical to use VALEN modelling to calibrate a measured signal to use as an estimated current. Each of the segments, then, is paired with a nearby measurement of loop voltage which, when coupled with an effective resistance of the segment as a whole, will provide an estimate of the total current in that segment. The current in each segment is distributed evenly throughout its cross-sectional area in the reconstruction. VALEN is used to compare predicted currents in the vessel segments for a few discharges to the loop voltage measurements, to calibrate the effective resistances to use for further equilibrium reconstructions. An example comparison is shown in Fig. 5 for poloidal field coil test discharge 23588 (no plasma) of the current in vessel segment 7U, above the outboard midplane (the upper half of the orange segment in Fig. 4a). Plotted are

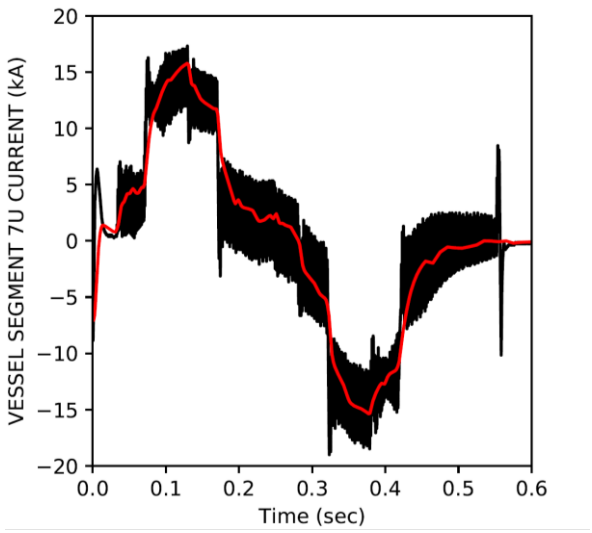


**Figure 5.** Comparison between measured loop voltage divided by effective resistance (black) and VALEN modelled (red) induced currents in the vessel segment 7U (above the outer midplane) during MAST poloidal field coil test discharge 23588.

the VALEN modelled current and the signal from loop voltage monitor P5U4 divided by the determined effective resistance of the segment, determined through this process to be $1.875\times10^{-5}$ Ohms. Good agreement is found.

## 4. Comparison of various levels of equilibrium reconstruction for MAST

Once the sources of current are included as described in the previous section, from both applied current in coils and estimated induced current in vessel structures, various levels of diagnostic data can be input, as described in section 2. As outlined in Ref. [19], a solution to fit the diagnostic data is iterated until a low convergence error is obtained. In this section, we show some examples of various quantities for MAST plasmas with the different levels of equilibrium reconstruction. For the magnetics only level, the available diagnostics were up to 16 loop voltage signals, 10 flux loops on the centre column and 36 spaced around the vessel poloidally, 40 centre column pickup coils measuring vertical field, and 19 pickup coils on the outboard side measuring vertical field and 19 measuring radial field. In practice, by the later stages of MAST operation, a number of those probes were broken, but plenty remained to provide a good magnetic reconstruction. In the kinetic reconstruction, 130 channels of Thomson scattering measurements of the electron temperature and density, as well as 64 channels of charge exchange recombination spectroscopy are added, as described in section 2.2. Finally, at the kinetic plus MSE level up to 35 channels of polarization angle from the MSE diagnostic are included, as described in section 2.3.

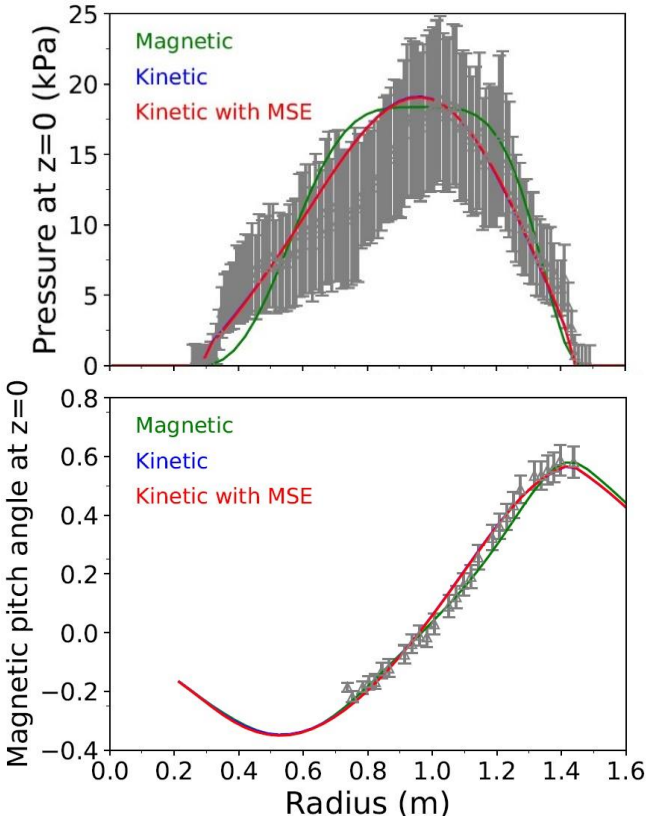


**Figure 6.** (top) Pressure and (bottom) magnetic pitch angle (in radians) profiles vs. radius at $z = 0$ for MAST discharge 23890 at 0.269 s. Three levels of equilibrium reconstruction are compared to the measured profiles (the pressure profile being partially measured and partially modelled).

Figure 6 shows a comparison of the reconstructed pressure and magnetic pitch angle profiles at the midplane from the three levels of reconstruction for an example case of MAST discharge 23890 at 0.269 s. This is the same discharge and time for which the flux surfaces were shown in Fig. 4a (from the kinetic plus MSE level). One can see differences in the profiles between the three levels of analysis. Note that the "measured" pressure profile is only partially measured, and partially modelled, as described in section 2.2. It is worth noting that while the Thomson scattering measurement of electron pressure spans the full midplane cross section of the plasma (in great detail, with 130 points), the charge exchange recombination spectroscopy measurement of the ion temperature spans from 0.78 m outward. The modelled data points for total pressure, shown in Fig. 6 with large error bars, therefore have two sections, one where $n_i$ and $p_f$ need to be assumed and another where additionally, $T_i$ is assumed (equal to $T_e$). These regions are not distinctly noticeable in Fig. 6, however, partly due to the large error bars.

We also note that the pressure profile was not available to the magnetics only reconstruction in green on the top panel of Fig. 6. Similarly, the MSE measured magnetic pitch angle data was

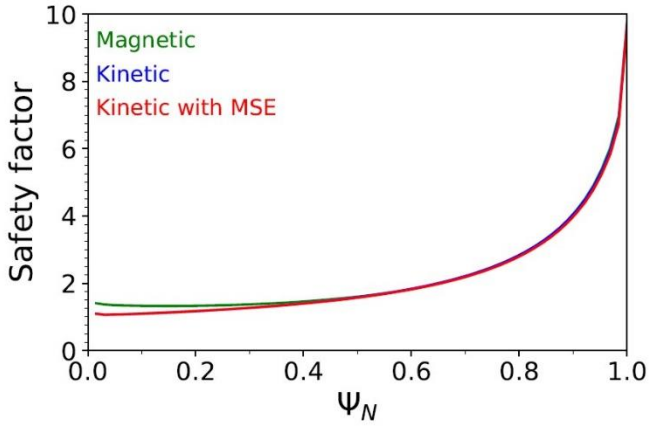


**Figure 7.** $q$ profile vs. normalized $\Psi$ for MAST discharge 23890 at 0.269 s.

not available to either the magnetic or kinetic reconstructions in the bottom panel. In spite of that, those levels of reconstruction actually do quite well compared to the MSE data already, before it is even included. The kinetic with MSE level of reconstruction actually does not further refine the kinetic profile in this case, because the kinetic reconstruction of pitch angle already fell within the error bars of the MSE measurement. Adding MSE data corroborates, but does not substantially change, the kinetic reconstructions. This can be seen as well in the $q$ profile for each level of reconstruction, shown in Fig. 7, vs. normalized $\Psi$. The $q$ profiles are all similar, but the kinetic cases differ slightly in the core where they have available measurements to constrain the fit but the magnetics only case does not. The two kinetic levels of reconstruction are almost identical throughout the discharge, as can be seen in Fig. 8, which shows the stored energy vs. time. At higher stored energy, the kinetic reconstructions show a somewhat lower value than the magnetics only case. It should be noted that the $q$ profile is monotonic in this case. It will also be useful to extend this analysis to equilibria with reversed shear $q$ profiles, where including the MSE data can have an increased impact upon the reconstructed $q$ profile (for example in Fig. 3 of Ref. [28]).

One method of determining how good the reconstruction is, is to examine the convergence error, $\mathrm{Max}|{\psi_n}^{m+1} - {\psi_n}^{m}|$, where $m$ is the iteration step [19]. The convergence error metric shows how well the equilibrium solution is converging to one solution, as opposed to bouncing between multiple solutions possible within the given constraints, for example. These are shown for MAST discharge 23890 vs. time in Fig. 8, including markers at time 0.269 s, when the profiles from Figs. 6 and 7 were taken from. The levels below $10^{-6}$ during the high stored energy part of the discharge are excellent. Additionally, the kinetic reconstructions are seen to perform better than the magnetics only during this portion of the

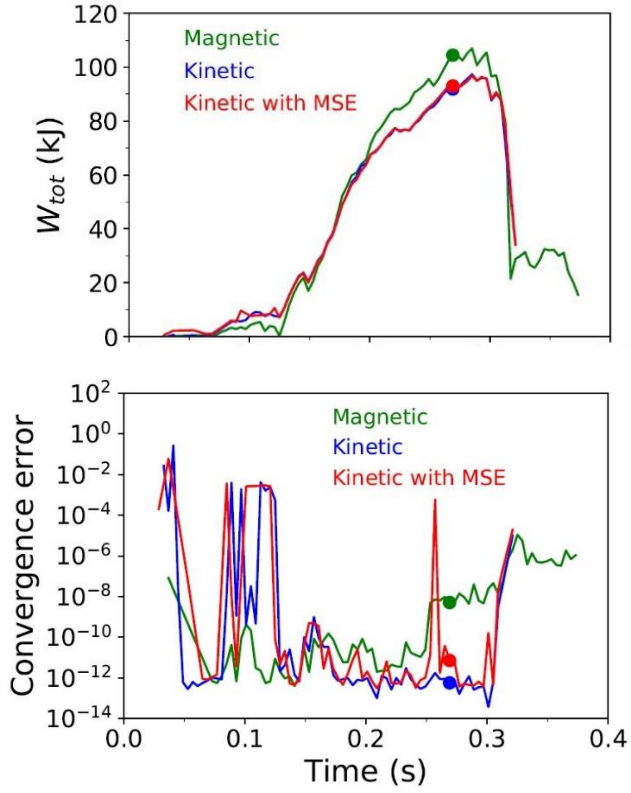


**Figure 8.** (top) Stored energy, and (bottom) convergence error vs. time for three levels of equilibrium reconstruction for MAST discharge 23890.

discharge. Adding MSE sometimes increases the convergence error in cases where the pressure and pitch angle constraints are not in perfect agreement.

Finally, an underlying assumption of the equilibrium reconstructions performed here is that the quantities are flux functions. Because the Thomson scattering measurements span the full cross section of the plasma, they can be used to check this assumption. Figure 9 shows the Thomson measurements of electron temperature mapped onto the normalized psi of the kinetic plus MSE reconstruction. In blue are the measurements on the inboard side and in red those on the outboard side. If the electron temperature is a flux function, these two sides should perfectly align. In this case they are quite close. It is possible to use a flux isotherm constraint in EFIT to enforce this condition [30], and in fact this will be required for reconstructions with rotation, but we have not as yet used that constraint here.

## 5. Initial analysis of the MAST database

In addition to the single equilibrium examples for MAST shown in the previous subsections, we have performed the same kinetic reconstruction analysis (with MSE) on many other discharges from the M7 and M8 experimental campaigns on MAST. Compiling a large database of kinetic equilibrium

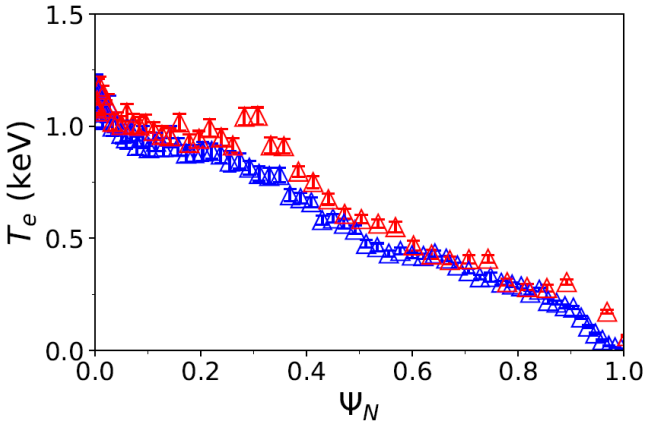


**Figure 9.** Thomson scattering $T_e$ profile vs. normalized **Ψ** for MAST discharge 23890 at 0.269 s, showing measurements on the inboard side ($R$<0.97m) in blue, and the outboard side ($R$>0.97m) in red.

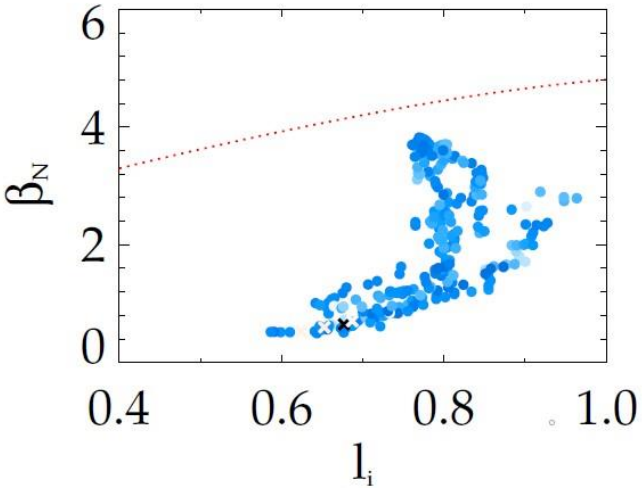


**Figure 10.** The calculated $\beta_N$ vs. $l_i$ stability space of plasmas in MAST. The blue colours indicate that nearly all equilibria have positive $\delta W$, below the no-wall limit. The dashed red line is the neural-net determined no-wall limit for NSTX.

reconstructions from the MAST database is valuable for many reasons. For example, they can be used as input for a neural network to predict density and pressure profile shapes [37], or in the disruption event characterization and forecasting (DECAF) code [38] database of multiple machine plasma disruptions. Additionally, a database of MAST equilibria will be useful to perform stability calculations of various types (as in Ref. [19] for KSTAR), including supplying input to a machine learning analysis of ideal magnetohydrodynamic (MHD) stability [3].

The ideal stability of MAST plasmas has been studied for individual or handfuls of discharges before [39,40,41,3]; the utility here is in compiling a large database. The no-wall beta limit has been explored for projected plasmas in MAST-U through artificial scans of pressure and $q$ profiles [4]. Here, the MAST database provides a natural scan of parameter space, rather than relying on theoretical scans that create combinations of profiles that may never be physically accessed in experiments. Even though it does not provide the full picture of global plasma stability [42], ideal stability calculations, for example knowledge of the no-wall beta limit, are important for tokamak operations, as they can be indicative of other plasma stability problems as well [43].

In the present work we will utilize the newly constructed database of MAST kinetic equilibrium reconstructions to test the capability of the DCON code [44] to determine the ideal stability of MAST plasmas. Ten different MAST discharges were used (23822, 23843, 23890, 24040, 24065, 24175, 24204, 24306, 24408, 24455). The kinetic equilibria with MSE generated in EFIT for these discharges were first fed through the CHEASE code [45] which, because it uses a prescribed plasma boundary, should reduce variability from time point to time point in the series of equilibria. The CHEASE output was then read in DCON, which determines the change in potential energy, $\delta W$, a negative value of which indicates the plasma is above the no-wall ideal MHD stability limit. Within each discharge the $\beta_N$ tended to increase with time and the pressure peaking decreased, but unfortunately $q_0$ also tended to decrease with time often going below 1 for the higher $\beta_N$ portions of the discharge. Since $q_0 < 1$ leads to untrustworthy calculations in DCON these times were discarded, leaving 275 time points between the 10 discharges.

Figure 10 shows the resulting calculations of the 275 equilibria plotted on a $\beta_N$ vs. $l_i$ plot. The colour of the points indicates their value of $\delta W$, with darker blue circles being more positive (more stable), lighter blue less stable, and red x's would indicate instability (see, for example, Fig. 1 from Ref. [42] for NSTX). In this case, however, practically all the points are stable, except for a couple of very light x's indicating a few calculations barely over the limit. This is not actually unexpected for MAST; in MAST the wall stabilization was quite weak, so the ideal *with*-wall limit was thought to be barely above the no-wall limit [4], and the practical implication of that was that plasmas in the MAST database should have very sparsely sampled the wall stabilized region of stability space. The dashed red line in Fig. 10 is the no-wall limit determined by a neural network for NSTX which showed possible indications of being useful for MAST as well [3]. All the equilibria calculated so far are below this limit. Specific effort will be required in future work to find MAST discharges in the database that can be used to refine the stability limit for MAST (higher $\beta_N$ with $q_0 > 1$), but the present study indicates that the kinetic equilibrium reconstructions produced so far are of sufficient quality for trustworthy stability calculations.

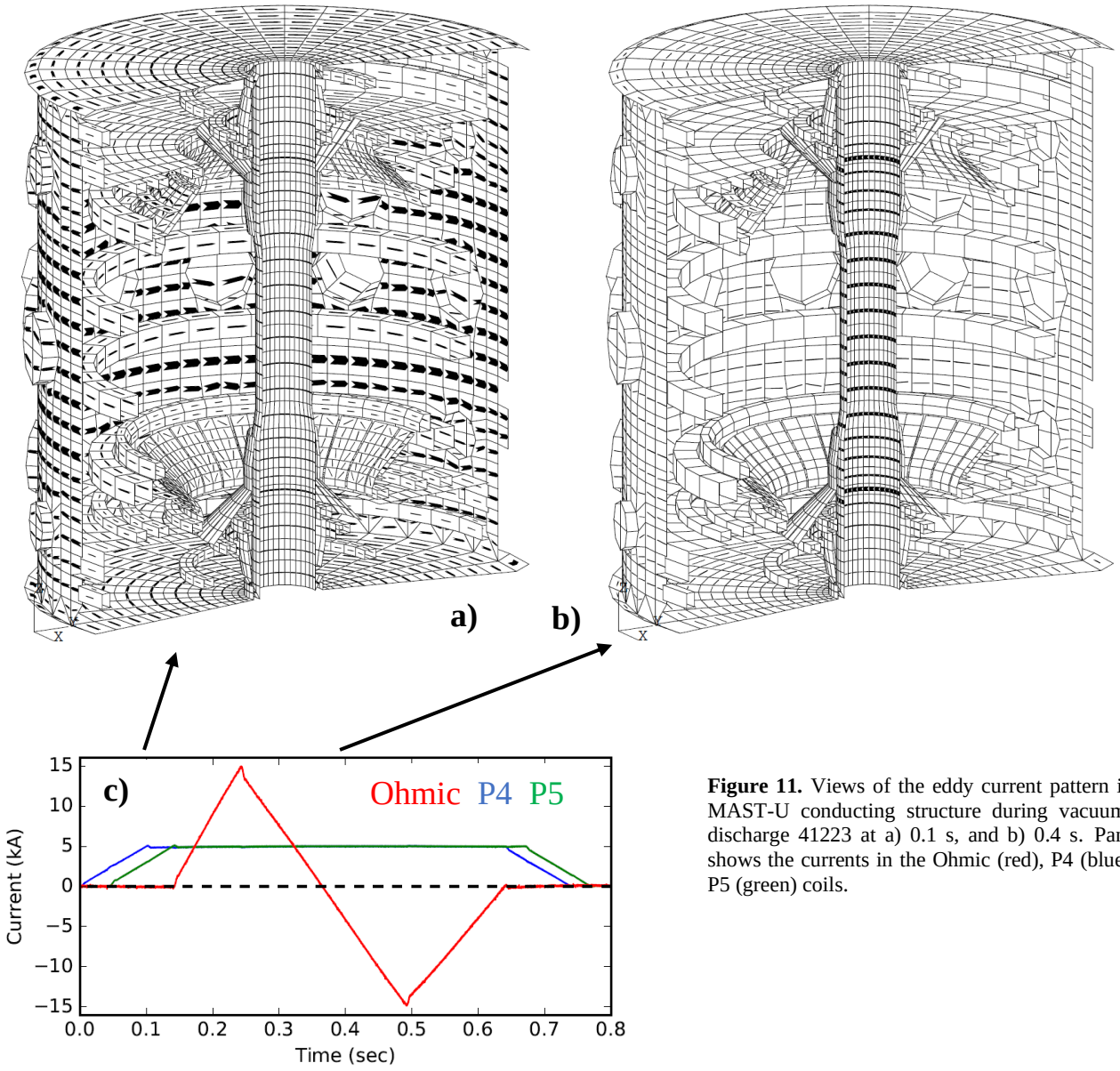


**Figure 11.** Views of the eddy current pattern in the MAST-U conducting structure during vacuum test discharge 41223 at a) 0.1 s, and b) 0.4 s. Panel c) shows the currents in the Ohmic (red), P4 (blue, and P5 (green) coils.

## 6. Preparation for equilibrium reconstruction of the first plasmas in MAST-U

The upgrade to MAST [2] was motivated by a desire to increase the plasma pulse length, heating power, current, and magnetic field, as well as to introduce a new advanced divertor configuration [46]. Naturally, these changes required changes in the machine, which means that the conducting structure in MAST-U is substantially different from that in MAST. Already it has been shown that the new conducting structure, in particular the stainless steel passive stabilisation plates (PSP), can impact the stability of the plasmas [4], as well as the start-up scenarios for plasma breakdown [47]. Of course, they will also impact reconstruction of the equilibrium. Like the VALEN model of the conducting structure used for MAST, the model for MAST-U is fully three dimensional, including all the ports in the vacuum vessel [4]. In the actual equilibrium reconstructions, also as in the MAST case, the vessel structures with estimated current are a reduced axisymmetric set of the structure. In Fig. 4b, the MAST-U conducting structure was shown in the same way as discussed for MAST in section 3. Also, like in the MAST case, VALEN is used to determine eddy currents in the 3D vessel structures for vacuum coil test shots. A diagram of the MAST-U conducting structure in VALEN [4], similar to Fig. 2 for MAST, is shown in Fig. 11. For MAST-U vacuum test discharge 41223, the Ohmic, P4, and P5 coils were tested, using the currents shown in Fig. 11c. At 0.1 s, during the P4 and P5 ramps, and before the Ohmic coil has current, the induced currents are mainly in the outer vacuum vessel and

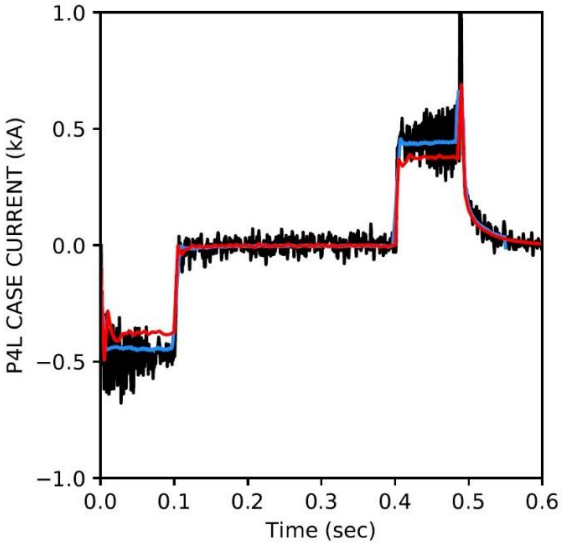


**Figure 12.** Comparison between measured (black) and VALEN (red) and EFIT++ (blue) modelled induced currents in the lower P4 coil case during MAST-U poloidal field coil test discharge 40315.

also the P4 and P5 coil cases (Fig. 11a). The total toroidal current in the vacuum vessel reaches about 90kA. Later, at 0.4 s, during the P4 and P5 flattops and during the Ohmic current swing, currents totalling almost 90kA are induced almost exclusively in the centre stack casing (Fig. 11b). In the plots, the arrows in each element are proportional to the current in that element, but they are rescaled between the time points so the largest arrow fits inside its element. There is almost twice as much current in the centre stack casing in the second plot as there is in the whole vessel in the first plot.

Like in the MAST case, the VALEN currents are mapped to effective resistances in the 2D vessel groupings in EFIT to be used in conjunction with nearby loop voltage measurements for estimated currents in the structures during reconstruction. In addition to the 3D VALEN model used in conjunction with the EFIT implementation of the present work, the EFIT++ code, which will also be used for MAST-U reconstructions, contains its own 2D conducting structure model.

First, analogously to Fig. 3 for MAST, the VALEN and EFIT++ models are tested by comparing between the modelled current in the coil cases and the measured current from Rogowski coils. Figure 12 shows this comparison, again for the P4 lower case, for MAST-U vacuum test discharge 40315, in which only the P4 coil was energized. There is considerable noise in the measured signal due to it actually being the difference between two large signals, the Rogowski measurements of the coil plus case currents minus the coil feed current. The comparison shows adequate, if not perfect, agreement, which should improve with further test discharges. This gives enough confidence in the models to again proceed to compare the conducting vessel segments shown in Fig. 4 with loop voltage measurements in order to determine effective resistances to use for equilibrium reconstructions.

Here, the PSP are again of particular interest because they are a new non-axisymmetric three dimensional structure that is quite close to the plasma surface. The connections between the individual plates span only half the plates height (see Fig. 13), and the resistivity of those connections is modelled, but not precisely known. If there is notable extra resistance due to the mechanical joint from plate to plate, eddy currents will be more likely to circulate within each plate. In other words, there will be a large current without a net toroidal component within each plate. On the other hand, if there is negligible extra resistance due to the mechanical joint (plate to plate) the sum total of all plates will act as a complete toroidal conductive path. This effect will be most important for periods of transient coil currents, less so at steady state. The effective resistance of the two dimensional EFIT vessel structure group that contains these actually three dimensional structures must be calibrated to accurately capture the effective 2D axisymmetric current resulting from the modelled 3D behaviour.

Figure 14 shows the comparison between the modelled induced currents in the upper passive stabilization plate structure during MAST-U poloidal field coil test discharge 40315, and a nearby loop voltage measurement divided by an effective resistance which is chosen so that current matches the VALEN model. This demonstrates that the VALEN model, as implemented, is able to capture the response of the PSP structures.

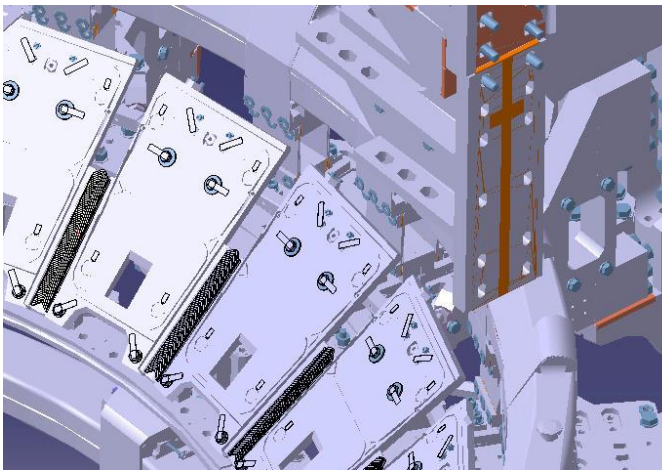

**Figure 13.** Diagram of the passive stabilization plates (PSP) in MAST-U, showing the gaps and connections between individual plates.

## 7. Conclusions

The necessary preparations for kinetic plasma equilibrium reconstructions are now established for the first operation of the MAST-U device. The three dimensional conducting structure has been implemented in the VALEN code and tested, demonstrating readiness for MAST-U reconstructions. The technique of using VALEN to determine eddy currents in the vessel structures during vacuum coil test shots and then using these to estimate currents in grouped vessel structures during the reconstruction of plasma discharges has been successfully established for a large database of discharges from MAST operation. Kinetic equilibrium reconstructions have been performed for this database in three levels: with magnetic measurements only, with magnetics and Thomson scattering measurements of electron temperature and density, charge exchange recombination spectroscopy measurements of ion temperature, and finally with those plus motional Stark effect (MSE) diagnosis of internal magnetic field pitch angle. The pitch angle data corroborates, but does not substantially change, the kinetic reconstructions; they matched the pitch angle measurements very well already before even including them in the reconstruction. Very low convergence errors were obtained for all discharges when the plasma stored energy was adequately high. Finally, the database of 275 MAST kinetic equilibrium reconstructions was used in DCON to calculate the ideal MHD stability in MAST. All discharges tested so far were below the no-wall limit; further analysis will be required.

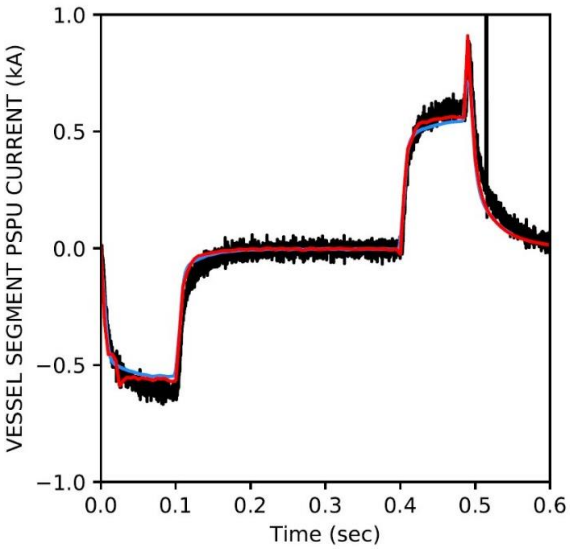


**Figure 14.** Comparison between measured loop voltage divided by effective resistance (black) and VALEN (red) and EFIT++ (blue) modelled induced currents in the upper passive stabilization plate structure during MAST-U poloidal field coil test discharge 40315.

## Acknowledgements

The authors acknowledge the invaluable help of R. Akers, L. Guazzotto, N. Hawkes, J. Hollocombe, A. Kirk, A. Piccione, D. Taylor, and A. Thornton. This research was supported by the U.S. Department of Energy under contracts DE-SC0018623 (Columbia University), and DE-AC02-09CH11466 (PPPL). This work is also partly funded by the RCUK Energy Programme [grant number EP/T012250/1] (CCFE) and by the Engineering and Physical Sciences Research Council [EP/L01663X/1] (Durham University). To obtain further information on the data and models underlying this paper please contact PublicationsManager@ukaea.uk.

## References

[1] Harrison J R *et al.* 2019 *Nuclear Fusion* **59** 112011
[2] Milnes J *et al.* 2015 *Fusion Engineering and Design* **96** 42
[3] Piccione A *et al.* 2020 *Nuclear Fusion* **60** 046033
[4] Berkery J W *et al.* 2020 *Plasma Physics and Controlled Fusion* **62** 085007
[5] Sabbagh S A *et al.* 2001 *Nuclear Fusion* **41** 1601
[6] Storrs J *et al.* 2006 *Fusion Engineering and Design* **81** 1841
[7] Eidietis N W *et al.* 2015 *Nuclear Fusion* **55** 063030
[8] Hole M J *et al.* 2005 *Plasma Physics and Controlled Fusion* **47** 581
[9] Chapman I T *et al.* 2010 *Nuclear Fusion* **50** 045007
[10] von Nessi G T *et al.* 2012 *Physics of Plasmas* **19** 012506
[11] Budny R V *et al.* 1992 *Nuclear Fusion* **32** 429
[12] Field A R *et al.* 2011 *Nuclear Fusion* **51** 063006
[13] van Wyk F *et al.* 2017 *Plasma Physics and Controlled Fusion* **59** 114003
[14] Cecconello M *et al.* 2019 *Nuclear Fusion* **59** 016006
[15] Lao L L *et al.* 1985 *Nuclear Fusion* **25** 1611
[16] Lao L L *et al.* 1990 *Nuclear Fusion* **30** 1035
[17] Lao L L *et al.* 2005 *Fusion Science and Technology* **48** 968
[18] Appel L *et al.* 2006 A unified approach to equilibrium reconstruction. In 33rd EPS Conference on Plasma Physics, Rome, 19 - 23 June 2006, Vol. 30I, P-2.184
[19] Jiang Y *et al.* (2020)
[20] Strait E J *et al.* 2008 *Fusion Science and Technology* **53** 304
[21] Edlington T *et al.* 2001 *Review of Scientific Instruments* **72** 421
[22] Scannell R *et al.* 2010 *Review of Scientific Instruments* **81** 10D520
[23] Gibson K J *et al.* 2010 *Plasma Physics and Controlled Fusion* **52** 124041
[24] Conway N J *et al.* 2006 *Review of Scientific Instruments* **77** 10F131
[25] Patel A *et al.* 2004 *Review of Scientific Instruments* **75** 4944
[26] Carpanese F *et al.* 2020 *Nuclear Fusion* **60** 066020
[27] Boyer M D *et al.* 2019 *Nuclear Fusion* **59** 056008
[28] Conway N J *et al.* 2010 *Review of Scientific Instruments* **81** 10D738
[29] De Bock M F M *et al.* 2012 *Plasma Physics and Controlled Fusion* **54** 025001
[30] Sabbagh S A *et al.* 2006 *Nuclear Fusion* **46** 635
[31] Fitzgerald M *et al.* 2013 *Nuclear Fusion* **53** 113040

[32] Guazzotto L *et al.* 2004 *Physics of Plasmas* **11** 604
[33] Guazzotto L *et al.* 2015 *Physics of Plasmas* **22** 092503
[34] Liu Y Q *et al.* 2020 *Nuclear Fusion* **60** 096026
[35] Bialek J M *et al.* 2001 *Physics of Plasmas* **8** 2170
[36] McArdle G J *et al.* 2008 *Fusion Engineering and Design* **83** 188
[37] Boyer M D *et al.* 2020 submitted to *Nuclear Fusion*
[38] Berkery J W *et al.* 2017 *Physics of Plasmas* **24** 056103
[39] Hole M J *et al.* 2005 *Plasma Physics and Controlled Fusion* **47** 581
[40] Chapman I T *et al.* 2011 *Nuclear Fusion* **51** 073040
[41] Chapman I T *et al.* 2011 *Plasma Physics and Controlled Fusion* **53** 065022
[42] Berkery J W *et al.* 2015 *Nuclear Fusion* **55** 123007
[43] Piovesan P *et al.* 2017 *Plasma Phys. Control. Fusion* **59** 014027
[44] Glasser A H 2016 *Phys. Plasmas* **23** 072505
[45] Lutjens H *et al.* 1996 *Comput. Phys. Commun.* **97** 219
[46] Morris W *et al.* 2018 *IEEE Transactions on Plasma Science* **46** 1217
[47] Battaglia D J *et al.* 2019 *Nuclear Fusion* **59** 126016